Prediction of Longitudinal Curvature Radius of 3D Surface Based on Quadratic Relationship between Strain and Coordinates in Continuous Roll Forming

Jiaxin Gao [1,2]**, Dongye He** [2,]*****, Lirong Sun** [1,2]**, Xi Zhang** [1,2] **and Zhongyi Cai** [1,2,]*****

[1] College of Materials Science and Engineering, Jilin University, Changchun 130025, China; gaojx1106@163.com (J.G.); sunlr92@163.com (L.S.); zhan9x1@126.com (X.Z.)

[2] Roll Forging Research Institute, Jilin University, Changchun 130025, China

***** Correspondence: hedy@jlu.edu.cn (D.H.); caizy@jlu.edu.cn (Z.C.); Tel.: +86-0431-8509-4340 (D.H. & Z.C.)

check for updates

Abstract: Continuous roll forming (CRF) is a new method for the rapid forming of three-dimensional (3D) surfaces developed in recent years, and the significant advantage of CRF compared with traditional die forming is that the longitudinal dimension of the sheet metal is not limited. By controlling the curvature radius and gap shape of upper and lower bending rolls, three-dimensional parts with different shapes and sizes can be precisely formed. When the elastic deformation is ignored during the forming process, the transversal curvature radius of the three-dimensional surface is consistent with the radius of the roll gap centerline. Therefore, the calculation of longitudinal curvature radius is the key to improve the accuracy of the 3D surface in CRF. In this paper, the basic principle of CRF is described. The modified formulas for calculating the longitudinal curvature radius of convex and saddle surfaces based on the quadratic relationship between the strain and coordinates are deduced in detail, and the corresponding design method of the roll gap is derived. Furthermore, the mathematical equations of convex and saddle surfaces are given. Through numerical simulation and theoretical analysis, it is found that the relative errors of the longitudinal centerline radius are reduced from 13.67% before modification to 4.35% after modification for a convex surface and 6.81% to 0.41% for a saddle surface when the transversal curvature radius is 800 mm and the compression ratio is 5%. The experimental and measured results indicate that the shapes of formed parts are more consistent with the target parts after modification, which further proves the applicability of the modified formulas.

Keywords: continuous roll forming; three-dimensional surface; curvature radius; numerical simulation; roll gap

1. Introduction

With the rapid development of manufacturing industry, the market demand for three-dimensional sheet metal is increasing. Automotive skins, hull outer panels, human skull prostheses, building plates and so forth are all composed of three-dimensional sheet metals with different shapes and sizes [1–4]. Single piece and small batch production is the current popular production mode. Obviously, due to the long manufacturing cycle, high maintenance cost and single production type, the application of traditional production is greatly limited. Instead, flexible forming has received more attention. The idea of multi-point flexible forming was proposed by Japanese scholars in the 20th century. In this process, the die surface with the same shape as the target surface is formed by controlling the closely arranged and height-adjustable basic units, and then the sheet is formed into a three-dimensional surface under the pressure of the die surface. Li et al. successfully applied multi-point technology to

actual production and combined it with traditional methods such as stretch forming [5–7]. However, when the size of the target part is large, more basic units are needed and this will lead to great processing cost. The continuous forming method is introduced so as to solve this problem. In the continuous forming process, a simple tool is used to gradually form the sheet into a desired shape. Rolling [8] and roll bending [9] are typical processes of continuous forming and are widely used at present. Yoon and Yang [10] tried to combine the idea of flexible forming and continuous forming in the early stage. They put forward the method of flexible incremental roll forming (FIRF), which uses the adjustable roll set including one upper center roll and two pairs of lower support rolls to form a three-dimensional curved surface. In order to improve the low efficiency of the FIRF process, Shim et al. [11] proposed a new technology called the line array roll set (LARS) process. This process uses three pairs of controllable rolls as forming tools, and each working roll is composed of several discrete small rolls. A doubly curved surface can be formed by one pass under the action of friction. Cai et al. [12–14] subsequently developed a continuous flexible forming (CFF) method, which greatly improved the forming quality of 3D curved surfaces.

In the last few years, Li et al. [15,16] advanced the CRF method to form 3D curved surfaces by applying flexible forming to rolling technology. The transversal bending of sheet metal is due to bending rolls, while the longitudinal bending is caused by the uneven thinning principle of rolling. The theory and formability of CRF have been studied deeply by researchers. Li et al. [17] studied the influence of different parameters such as reduction, forming velocity and friction on the shape of formed parts. Ku et al. [18] proposed the NURBS control method to determine the roll gap distribution. Liu et al. [19] suggested that adding two auxiliary rolls to the original two work rolls would make the forming process more stable. Park et al. [20] established a regression model and an artificial neural network model to predict the longitudinal curvature radius, and it was found that the regression model is more suitable for the prediction of convex parts, and the artificial neural network model is more suitable for the prediction of saddle parts. Ghiabakloo et al. [21] used the finite element method and genetic algorithm to calculate the longitudinal curvature radius. Cai et al. [22–24] analyzed the mechanism of the longitudinal bending deformation of the sheet metal from a mechanics perspective, and put forward the necessary condition of CRF; that is, the longitudinal strain is the first-order function of coordinates. Based on this condition, the calculation formula of the longitudinal curvature was derived. In order to improve the prediction accuracy and facilitate practical application, a new method for predicting the longitudinal curvature radius of 3D surface based on the quadratic relationship between the strain and coordinates is proposed in this paper.

This work reports on the further investigation for prediction of longitudinal curvature radius after the previous research [22–24] studied by Cai et al. In this study, the principle of CRF is explained, and the cause of longitudinal bending of sheet metal is further analyzed. The previous argument that the longitudinal strain is a linear function of coordinates is extended to the argument of this paper that the longitudinal strain is a quadratic function of coordinates. Based on this point of view, the original formula for calculating the longitudinal curvature radius of sheet metal is modified in the range of transversal curvature radii of 800~1000 mm and compression ratios of 3~7%. The design method of the roll gap for a three-dimensional surface is proposed according to the new formulas. In addition, the mathematical equations for convex and saddle surfaces are given. Through numerical simulation and experimental analysis, it is found that the prediction accuracy of longitudinal curvature radius is greatly improved after the formula is modified.

2. Forming Theory of CRF Based on Two Bending Rolls

2.1. Continuous Roll Forming Process

The most important tool for CRF is a pair of small diameter work rolls with low bending rigidity and high torsional rigidity. They are straight in their free state and can be slightly bent by external force [17]. Under the control of shape-adjusting and supporting assembly, the work rolls can maintain

the bending state and rotate around their own axes. In the CRF process, the flat sheet metal is turned into a three-dimensional sheet with certain curvatures in both transversal and longitudinal directions by controlling the bending profiles of upper and lower work rolls and the roll gap size. In order to form an uneven gap which is the key to the three-dimensional surface forming, the bending profiles of the two rolls should be a little different. Due to the large plastic deformation during the rolling process, the effect of elastic deformation can be ignored. Therefore, the curvature radius of the roll gap centerline is the same as the transversal curvature radius of the target. The longitudinal curvature is formed by the non-uniform roll gap. When the roll gap is small in the middle and large on both sides, the sheet metal is bent upward to form a convex part with positive Gaussian curvature [19]. When the roll gap is uniform, the deformation process degenerates into a normal rolling process and a cylindrical part with zero Gaussian curvature (2D surface) is formed. Furthermore, when the roll gap is small on both sides and large in the middle, a saddle part with negative Gaussian curvature is formed, as shown in Figure 1.
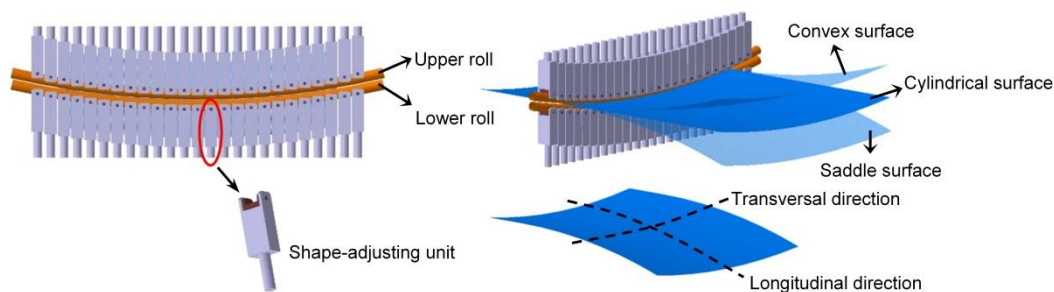

Figure 1. Schematic diagram of continuous roll forming.

Figure 2 shows the process of continuous roll forming. First, the bending radii of upper and lower rolls are adjusted according to the transversal curvature radius of the target surface, and the sheet to be formed is placed between the two rolls. Then, the upper roll moves vertically downward, and the lower roll remains stationary, thereby forming an uneven roll gap. Next, the two work rolls rotate reversely around their own bending axes at the same angular speed. The sheet metal is continuously formed under the effect of rolling force and friction, and finally becomes a three-dimensional surface with double curvatures.
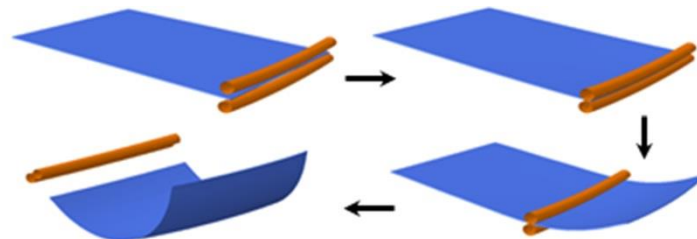

Figure 2. Continuous roll forming process.

2.2. Theoretical Model and Formulas Derivation of CRF

The theoretical model and formulas derived in this paper are based on the following conditions: (1) because of the large plastic deformation in the rolling process, the influence of elastic deformation is ignored; (2) the thickness of the sheet is much smaller than the width, so the strain in the width direction is ignored, and the strain in the thickness direction is thought to be uniformly distributed. Therefore, the continuous roll forming can be treated as a plane strain problem [16]; (3) it is considered that the deformation process no longer follows the plane assumption, that is, the plane cross section becomes a curved surface after deformation. Figure 3 is the illustration of roll gap at the exit section. The size of the roll gap (Ω_g) at different positions is expressed in $h(v)$, where v is the parameter

coordinate in the transversal direction. In order to facilitate the analysis, the centerline of the roll gap described by $z = g(v)$ is simplified as an arc, and the radius of the arc is indicated by ρ_T. The longitudinal curvature of three-dimensional sheet metal at different position is denoted by $\rho_l^{-1}(v)$, and $\rho_L = \rho_l(v)|_{v=0}$. Furthermore, ρ_T and ρ_L are the principal curvature radii in the transversal and longitudinal directions, respectively.

The previous formulas are derived based on plane assumption [16,23], and the longitudinal strain is divided into membrane strain and bending strain. The longitudinal strain ε_l can be denoted as

$$\varepsilon_l = a_0 + a_1 y + a_2 z \quad (y, z \in \Omega_g) \tag{1}$$

From Equation (1), a_0, a_1 and a_2 can be easily found [23,24], that is

$$\begin{cases} a_0 = \varepsilon_m - a_1 y_0 - a_2 z_0 \\ a_1 = \rho_l^{-1} \sin \alpha \\ a_2 = \rho_l^{-1} \cos \alpha \end{cases} \tag{2}$$

where $y_0 = \int_{\Omega_g} y dA / \int_{\Omega_g} dA$, $z_0 = \int_{\Omega_g} z dA / \int_{\Omega_g} dA$, and α is the angle between the bending neutral axis and the y-axis.

The expression of membrane strain is

$$\varepsilon_m = \int_A \varepsilon_l dA / A \tag{3}$$

where A is the area of the roll gap.

When the roll gap is symmetrical about the z-axis, $\alpha = 0$. Thus, Equation (1) can be written as

$$\varepsilon_l = a_0 + \rho_l^{-1} z (y, z \in \Omega_g) \tag{4}$$

According to Equation (4), the longitudinal strain is a linear function of height coordinate z. The constant term is the membrane strain, which represents the overall translation of the cross section. The first-order term is the bending strain representing the overall rotation of the cross section around the neutral axis. The slope of $\varepsilon_l - z$ line is the longitudinal curvature of the three-dimensional surface. It can be seen that the longitudinal curvature calculated by Equation (4) is a fixed value. However, for a three-dimensional surface formed by continuous roll forming, the longitudinal curvature varies at different positions of the cross section, so the formula derived in view of plane assumption has a large error in most cases. On this basis, the formula is modified in this paper. The longitudinal curvature is assumed to be a linear function varying with the coordinates rather than a constant, and then more practical formulas are deduced.
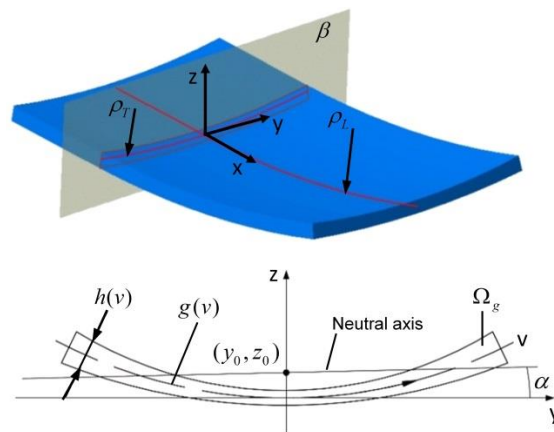

Figure 3. Illustration of the roll gap.

2.3. Modification of the Formula for Calculating the Longitudinal Curvature Radius of Convex Surface

For convex surface before modification, the longitudinal strain is a linear subtraction function of the height coordinate, as shown in the black dotted line in Figure 4. Subscript e represents a convex surface. Thus, Equation (4) can be written as

$$\varepsilon_{le} = \varepsilon_{max} - \frac{1}{\rho_l}z \tag{5}$$

Suppose that the longitudinal curvature is a linear function of the height coordinate, that is

$$\rho_{le}{}^{-1}(v) = bz + c \tag{6}$$

Taking Equation (6) into Equation (5), the expression of longitudinal strain can be denoted by

$$\varepsilon_{le} = -bz^2 - cz + \varepsilon_{max} \tag{7}$$

The relationship between the longitudinal curvature and the longitudinal strain can be expressed as

$$\rho_{le}{}^{-1}(v) = -\frac{1}{2}\varepsilon_{le}{}' + \frac{1}{2}c \tag{8}$$

It can be seen from Equation (7) that the longitudinal strain is a quadratic function of the height coordinate, which shows that the plane assumption is not tenable. The longitudinal strain can not only be divided into membrane strain and bending strain, but also includes a secondary compensation strain, which together with the first-order bending strain determines the longitudinal bending of surfaces. The $\varepsilon_{le} - z$ curve is shown as a black solid line in Figure 4. On the cross section of sheet metal, the maximum strain difference and the maximum height difference are given by

$$\begin{cases} \varepsilon_d = \varepsilon_{max} - \varepsilon_{min} \\ z_d = z_{max} - z_{min} \end{cases} \tag{9}$$

where ε_{max} and ε_{min} are the maximum and minimum values of longitudinal strain on the cross section, respectively.

The point on the symmetry axis of quadratic function curve is a characteristic point. The symmetry axis of the $\varepsilon_{le} - z$ curve is represented by $z = nz_d (n < 0)$.
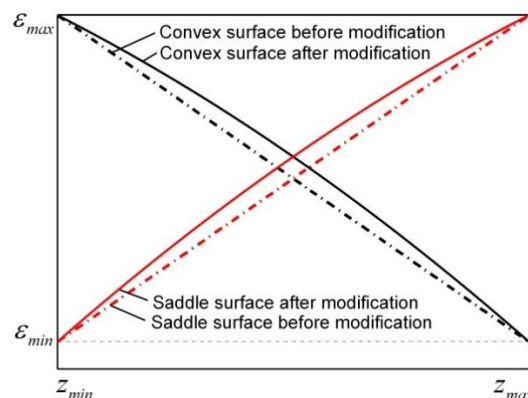

Figure 4. Relationship between longitudinal strain and height coordinate.

For convex surfaces, the longitudinal curvature radius at the center of the sheet metal is the largest, and the closer to the edge, the smaller the longitudinal curvature radius. Therefore, $b > 0$ and $c > 0$ can be inferred. The longitudinal strain at the center and edge are expressed as

$$\begin{cases} \varepsilon_{le} = \varepsilon_{max}, & z = z_{min} = 0 \\ \varepsilon_{le} = \varepsilon_{min}, & z = z_{max} = \rho_T(1 - \cos\theta_0) \end{cases} \tag{10}$$

where θ_0 is the longitudinal bending angle.

From Equation (7) to Equation (10), the parameters b and c can be solved as follows:

$$\begin{cases} b = -\dfrac{\varepsilon_d}{(2n-1)z_d{}^2} \\ c = \dfrac{2n\varepsilon_d}{(2n-1)z_d} \end{cases} \tag{11}$$

Substituting Equation (11) into Equation (7), the longitudinal strain can be written as

$$\varepsilon_{le} = \frac{\varepsilon_d}{(2n-1)z_d{}^2}z^2 - \frac{2n\varepsilon_d}{(2n-1)z_d}z + \varepsilon_{max} \tag{12}$$

At the same time, the longitudinal curvature radius can be obtained by

$$\rho_{le}(v) = \frac{2nz_d - z_d}{2nz_d - z}\rho_l{}^* \tag{13}$$

where $\rho_l{}^* = z_d/\varepsilon_d$ is the expression of the longitudinal curvature radius before correction.

The longitudinal curvature radius at $z = 0$ can be expressed as

$$\rho_L = (1 - \frac{1}{2n})\rho_l{}^* \tag{14}$$

To determine the value of n, a large number of numerical simulations have been carried out on convex surfaces. The transversal curvature radii are taken as 800~1000 mm, and the compression ratios are taken as 3~7%. The curvature radius of the longitudinal centerline ρ_L is measured and the longitudinal radius before correction $\rho_l{}^*$ is calculated. It is found that the ratio of the two is close to a constant under the condition of different compression ratios and transversal curvature radii. Let k_e be the ratio, then $k_e = 1.110$ is determined through numerical simulation and calculation, as shown in the black solid line in Figure 5. The compression ratio is expressed as δ. Thus, the value of n is determined as −4.55. Substituting n into Equations (12) and (13), the calculation formulas of longitudinal strain and longitudinal curvature radius under the condition of transversal curvature radii of 800~1000 mm and compression ratios of 3~7% are as follows:

$$\varepsilon_{le} = -0.099\frac{\varepsilon_d}{z_d{}^2}z^2 - 0.901\frac{\varepsilon_d}{z_d}z + \varepsilon_{max} \tag{15}$$

$$\rho_{le}(v) = \frac{z_d}{0.901z_d + 0.099z}\rho_l{}^* \tag{16}$$

Neglecting the strain in the width direction and elastic deformation, together combining with the volume invariance law of plastic deformation, the roll gap can be expressed as

$$h(v) = H\exp(-\varepsilon_l) \tag{17}$$

where H is the original thickness of the sheet.

Taking Equation (15) into Equation (17), the expression of the roll gap for convex surface is as follows:

$$h_e(v) = H\exp(0.099\frac{\varepsilon_d}{z_d{}^2}z^2 + 0.901\frac{\varepsilon_d}{z_d}z - \varepsilon_{max}) \tag{18}$$
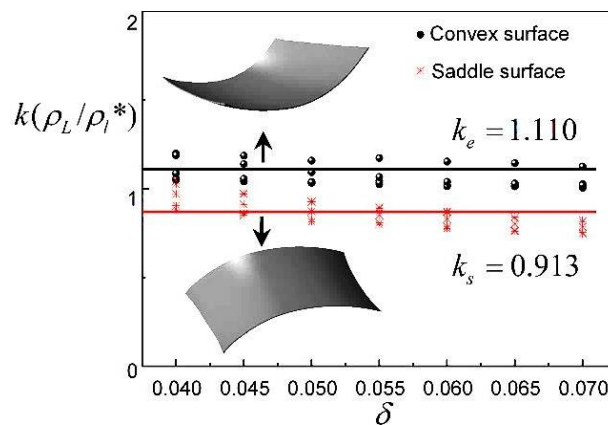
Figure 5. Ratio of simulation values to uncorrected calculated values.

2.4. Modification of the Formula for Calculating the Longitudinal Curvature Radius of Saddle Surface

Before modification, the longitudinal strain of a saddle surface is a linear increasing function of the height coordinate, as shown by the red dotted line in Figure 4. Subscript s represents the saddle surface. Thus, Equation (4) can be rewritten as

$$\varepsilon_{ls} = \varepsilon_{min} + \frac{1}{\rho_l}z \tag{19}$$

It is still assumed that the longitudinal curvature of saddle surface is a linear function of the z coordinate, which can be denoted by

$$\rho_{ls}{}^{-1}(v) = pz + q \tag{20}$$

Therefore, the expression of longitudinal strain is

$$\varepsilon_{ls} = pz^2 + qz + \varepsilon_{min} \tag{21}$$

For saddle-shaped surfaces, the relationship between the longitudinal strain and the longitudinal curvature can be expressed as

$$\rho_{ls}{}^{-1}(v) = \frac{1}{2}\varepsilon_{ls}' + \frac{1}{2}q \tag{22}$$

The actual $\varepsilon_{ls} - z$ curve is shown as a red solid line in Figure 4. Let the symmetry axis of $\varepsilon_{ls} - z$ curve be $z = mz_d (m > 0)$.

The longitudinal curvature radius at the center of saddle surface is the smallest, and the closer to the edge of the sheet, the greater the longitudinal curvature radius. Hence, it can be inferred that $p < 0$ and $q > 0$. The longitudinal strain at the center and edge of the sheet metal is given as

$$\begin{cases} \varepsilon_{ls} = \varepsilon_{min}, & z = z_{min} = 0 \\ \varepsilon_{ls} = \varepsilon_{max}, & z = z_{max} = \rho_T(1 - \cos\theta_0) \end{cases} \tag{23}$$

From Equation (21) to Equation (23), it is found that the expressions of p and q can be written as follows:

$$\begin{cases} p = -\dfrac{\varepsilon_d}{(2m-1)z_d{}^2} \\ q = \dfrac{2m\varepsilon_d}{(2m-1)z_d} \end{cases} \tag{24}$$

Thus, the longitudinal strain and curvature radius can be given by

$$\varepsilon_{ls} = -\frac{\varepsilon_d}{(2m-1)z_d{}^2}z^2 + \frac{2m\varepsilon_d}{(2m-1)z_d}z + \varepsilon_{min} \tag{25}$$

$$\rho_{ls}(v) = \frac{2mz_d - z_d}{2mz_d - z}\rho_l^*$$ (26)

The longitudinal curvature radius at $z = 0$ for saddle surface can be expressed as

$$\rho_L == (1 - \frac{1}{2m})\rho_l^*$$ (27)

A lot of numerical simulations are carried out by setting the transversal curvature radii of saddle surface as 800~1000 mm and the compression ratios as 3~7%. The radius of the longitudinal centerline ρ_L is measured and the theoretical value ρ_l^* is calculated using the formula before modification. Let k_s be the ratio of ρ_L and ρ_l^*, and it is found that k_s is close to a constant of 0.913 under different transversal curvature radii and compression ratios, as shown in the red solid line in Figure 5. Thus, it can be inferred that $m = 5.75$. Therefore, the final expressions of longitudinal strain and longitudinal curvature radius for saddle surface under the condition of transversal curvature radii of 800~1000 mm and compression ratios of 3~7% can be expressed as

$$\varepsilon_{ls} = -0.095\frac{\varepsilon_d}{z_d^2}z^2 + 1.095\frac{\varepsilon_d}{z_d}z + \varepsilon_{min}$$ (28)

$$\rho_{ls}(v) = \frac{z_d}{1.095z_d - 0.095z}\rho_l^*$$ (29)

Taking Equation (28) into Equation (17), the formula of roll gap for saddle surface can be given as follows:

$$h_s(v) = H\exp(0.095\frac{\varepsilon_d}{z_d^2}z^2 - 1.095\frac{\varepsilon_d}{z_d}z - \varepsilon_{min})$$ (30)

3. Numerical Simulations for Convex and Saddle Surfaces

3.1. Finite Element Model

In order to verify the applicability of the modified formulas of longitudinal curvature radius, the finite element models of convex and saddle surfaces are established by ABAQUS/explicit software, and the relevant explicit dynamic analysis is carried out. It can be seen from Figure 6 that the upper and lower work rolls are composed of segmented small rigid rolls, and a local coordinate system is established for each rigid roll to ensure that the bending rolls can rotate around their own axes. Each small roll with a radius of 7.5 mm and a width of 6 mm is meshed using bilinear quadrilateral three-dimensional rigid element with four nodes, and the size of each unit is 0.5 mm × 0.5 mm. The length, width and thickness of the sheet to be formed are 300, 270, and 2 mm, respectively, and the material used in the simulation is 08 AL. The mechanical properties of 08 AL shown in Table 1 are determined by the uniaxial tensile test. It is considered that the material follows Mises yield criterion and conforms to the elastoplastic constitutive relationship with isotropic hardening. The friction coefficient is taken as 0.2. For the purpose of making the results more accurate, the C3D8R element is used to mesh the sheet metal. A large number of simulation results show that although the sheet metal is a deformable body, the forming effect is better when its element size is larger than that of the rigid work roll, so the element size of the sheet metal is set as 1.5 mm × 1.5 mm × 1 mm. Since the thickness of the sheet is small, the strain value of each point in the cross section can be accurately captured by using two elements in the thickness direction. In order to save computing resources, considering the symmetry of the model, only 1/2 of the finite element model is established for calculation and analysis.

The difference between the finite element models of convex surface and saddle surface is only that the roll gap is not the same. As mentioned before, the roll gap is small in the middle and large on both sides for a convex surface, while the distribution of the roll gap for a saddle surface is the opposite. Before and after the modification of the calculation formula of the longitudinal curvature radius, the size of the roll gap changes slightly, as shown in Figure 7. Cases 1–3 are for convex surfaces and Case 4 is for saddle surfaces.
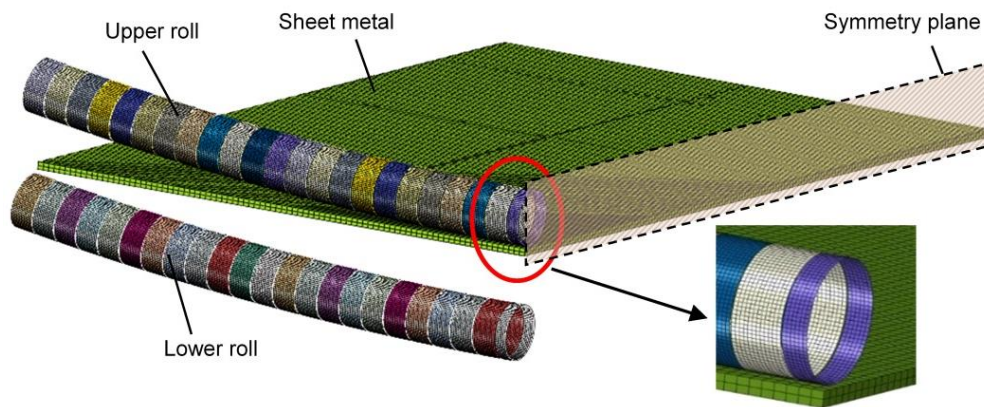
Figure 6. Finite element model.

Table 1. Mechanical properties of 08 AL.

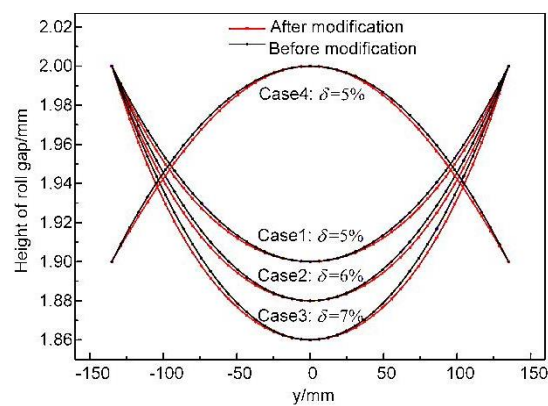| Material	Density (kg/m^3)	Poisson's Ratio	Elastic Modulus (GPa)	Yield Strength (MPa)
08 AL	7845	0.29	207	91.294

Figure 7. Height of roll gap for convex and saddle surfaces.

3.2. Simulation Results and Analysis for Convex Surface

In this study, the forming results of convex surfaces with a transversal curvature radius of $\rho_T = 800$ mm and compression ratios of 5%, 6% and 7% are analyzed. The equation of the formed convex surface can be expressed as

$$S_e(u,v) = \left\{ \begin{array}{c} \left\{ \rho_L - \rho_T\left[\left(1 - \cos(\frac{v}{\rho_T})\right)\right] \right\} \sin(\frac{u}{\rho_L}) \\ \rho_T \sin(\frac{v}{\rho_T}) \\ \rho_L - \left\{ \rho_L - \rho_T\left[\left(1 - \cos(\frac{v}{\rho_T})\right)\right] \right\} \cos(\frac{u}{\rho_L}) \end{array} \right\} \tag{31}$$
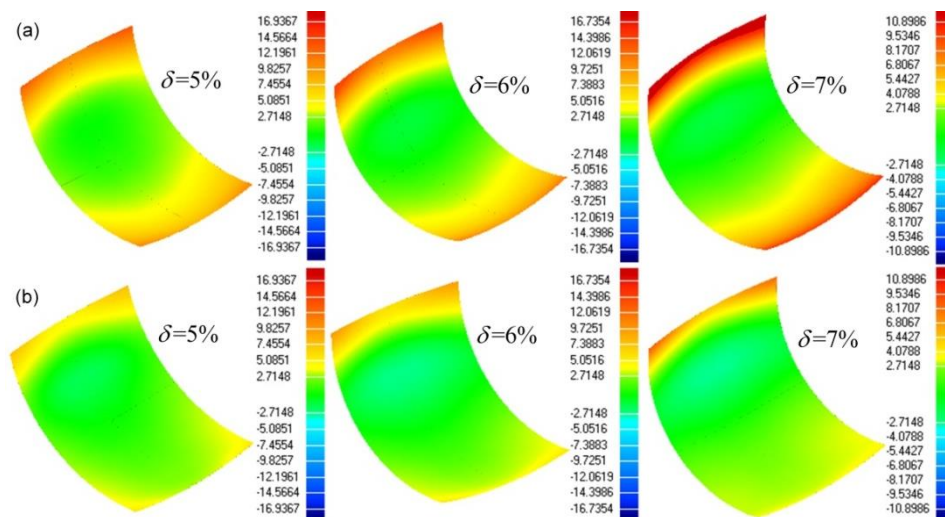
where u is the parameter coordinate in the longitudinal direction.

The theoretical values of longitudinal curvature radius are calculated by the formula before and after correction, respectively, and compared with the actual forming results. The results are shown in Table 2.

Table 2. Error comparison of longitudinal curvature radius for convex surface.

δ	z/mm	Before Modification			After Modification		
		Calculated Value/mm	Simulated Value/mm	Error	Calculated Value/mm	Simulated Value/mm	Error
0.05	0	227.46	263.48	13.67%	252.45	263.94	4.35%
0.05	5.74	221.73	256.78	13.65%	239.31	256.58	6.73%
0.05	11.47	215.99	252.41	14.43%	227.46	248.16	8.34%
0.06	0	189.21	218.13	13.26%	209.99	222.23	5.50%
0.06	5.74	183.47	211.60	13.29%	199.06	211.41	5.84%
0.06	11.47	177.74	208.32	14.68%	189.21	207.30	8.73%
0.07	0	161.88	182.12	11.11%	179.67	186.16	3.49%
0.07	5.74	156.15	179.36	12.94%	170.31	180.35	5.56%
0.07	11.47	150.41	176.18	14.63%	161.88	175.91	7.97%

It can be seen from Table 2 that the relative error after correction is significantly reduced compared with that before correction, and the error of each position of the surface is controlled within 9%, which indicates that the corrected formula is more in line with the actual forming results. Figure 8 shows the error nephograms under different compression ratios (δ). Both before and after the correction, the error at the end region of the convex surface formed by continuous roll forming is significantly greater than that at the middle region, which is caused by the straight edge effect. Specifically, the longitudinal bending of sheet metal is the result of the interaction of longitudinal stresses with different magnitude in the transversal direction. At the beginning and end of forming, due to the law of minimum resistance, the metal in the stressed area flows to the respective adjacent end, so that the interaction of longitudinal stresses is not enough to make both ends of sheet metal reach the bending degree of the middle region.

Figure 8. Error nephograms under different compression ratios (δ) of convex surfaces: (a) Before modification; (b) After modification.

The simulated convex surfaces deviate from the target to a large extent before modification, and the modified formula makes the shape and size of the formed surfaces more consistent with the target, as shown in Figure 8, in which the proportion of the green area of the surfaces increases obviously. In addition, it is found that the longitudinal curvature radius decreases with the increase in the compression ratio, which can be explained by the modified Formula (16). With the increase in compression ratio, the longitudinal strain difference ε_d between the center and the edge of the sheet increases and a smaller ρ_{l*} is obtained, thus the longitudinal curvature radius decreases.

In order to verify the relationship between strain and coordinate, the z-coordinate and longitudinal strain values of each node on the transversal centerline of the convex surface before and after modification are extracted, as shown in Figure 9a. Since the roll gap has little change before and after correction, the strain before and after correction is very close when the compression ratio is the same. The strain points in the diagram are distributed near the blue quadratic curve, which proves that the strain is indeed a quadratic function of coordinates.
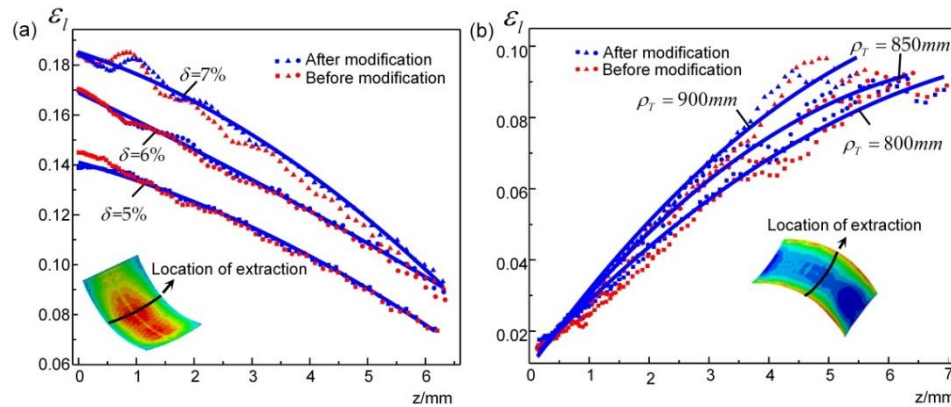

Figure 9. Relationship between longitudinal strain and z-coordinate obtained from numerical simulation: (**a**) convex surface; (**b**) saddle surface.

3.3. Simulation Results and Analysis for Saddle Surface

The formation of saddle surfaces with a compression ratio of 5% and transversal curvature radii of 800, 850 and 900 mm are studied. The equation for the target saddle surface can be written as

$$
S_s(u,v) = \left\{
\begin{array}{l}
\left\{\rho_L + \rho_T\left[(1 - \cos(\frac{v}{\rho_T}))\right]\right\} \sin(\frac{u}{\rho_L}) \\
\rho_T \sin(\frac{v}{\rho_T}) \\
\left\{\rho_L + \rho_T\left[(1 - \cos(\frac{v}{\rho_T}))\right]\right\} \cos(\frac{u}{\rho_L}) - \rho_L
\end{array}
\right\}
\tag{32}
$$

The theoretical values of the longitudinal curvature radius of saddle surfaces before and after correction are calculated and compared with the values obtained from the simulation. The results are shown in Table 3.

Table 3. Error comparison of longitudinal curvature radius for saddle surface.

Transversal Radius/mm	z/mm	Before Modification			After Modification		
		Calculated Value/mm	Simulated Value/mm	Error	Calculated Value/mm	Simulated Value/mm	Error
800	0	227.46	212.97	6.81%	207.73	208.58	0.41%
800	5.74	233.20	219.00	6.48%	217.15	215.84	0.61%
800	11.47	238.93	224.78	6.30%	227.46	221.70	2.60%
850	0	213.91	199.89	7.02%	195.35	194.81	0.28%
850	5.39	219.30	205.51	6.71%	204.21	201.76	1.21%
850	10.79	224.70	210.79	6.60%	213.91	208.43	2.63%
900	0	201.89	177.83	13.53%	184.37	172.59	6.83%
900	5.09	206.98	183.69	12.68%	192.73	181.52	6.18%
900	10.18	212.07	188.06	12.76%	201.89	188.13	7.31%

Due to the slight difference in roll gap, the simulated longitudinal curvature radius of saddle surfaces after correction is different from that before correction, but the change is small. From Table 3, it can be seen that the relative error of the longitudinal curvature radius is evidently reduced after correction, from the original 6.30~13.53% to 0.28~7.31%. Figure 10 shows the error nephograms

under different transversal curvature radii, indicating the error change more intuitively. As shown in Figure 10, saddle surfaces also have a straight edge effect. The modified saddle surface is closer to the target, and this can significantly increase the material utilization. With the increase in the transversal curvature radius, the longitudinal curvature radius decreases correspondingly, which can be explained by the modified Formula (29) as follows: the larger the transversal curvature radius is, the smaller the height difference z_d between the center and the edge of the sheet metal is, thus the smaller the longitudinal curvature radius is. Figure 9b shows that the strain is a quadratic function of coordinates for saddle surface. Due to the small change in roll gap, the strain before and after modification is very close. The strain points under each transversal curvature radius are distributed near the blue quadratic curve. Therefore, there is a certain error in calculating the longitudinal curvature radius by using the linear relationship between strain and coordinates before modification.
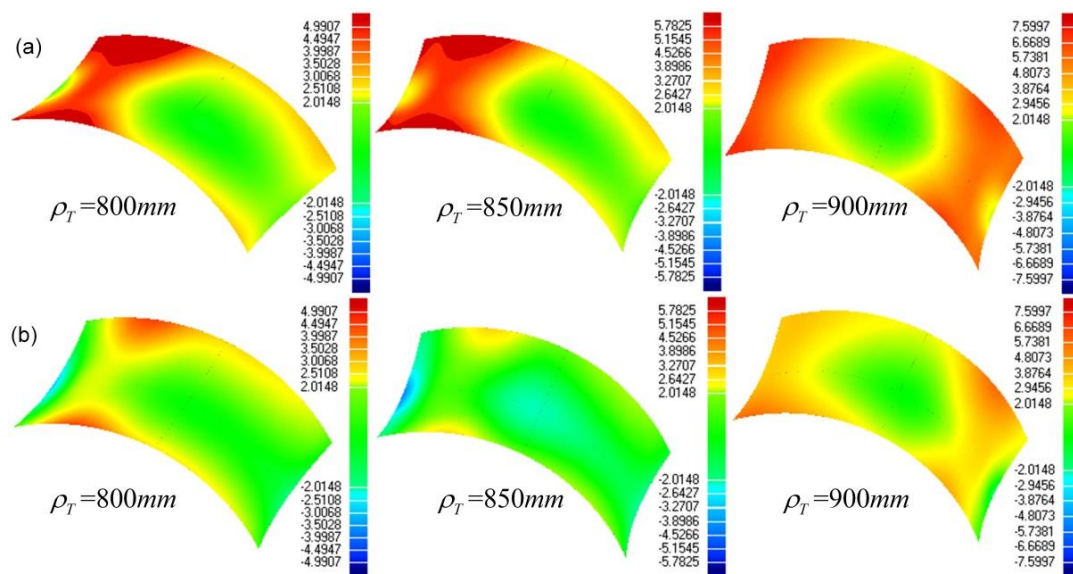

Figure 10. Error nephograms under different transversal radii of saddle surfaces: (**a**) before modification; (**b**) after modification.

The simulations of convex and saddle surfaces show that the modified formulas are more suitable for continuous roll forming. If the transversal curvature and longitudinal curvature of the three-dimensional surface are given for CRF, the ideal surface can be obtained by the following steps. First, adjust the centerline radius of the roll gap to the transversal curvature radius of the target surface, and then calculate the size of the roll gap according to the Equation (18) or Equation (30) to control the position of the upper and lower work rolls. Finally, continuous rolling is carried out in order to get the ideal surface.

4. Experimental Verifications

4.1. Experimental Equipment of CRF

The experimental equipment for continuous roll forming is shown in Figure 11. There are 31 shape adjusting units on the top and bottom of the equipment, respectively, which are used to adjust the bending shapes of the work rolls and keep the shapes unchanged during the process. The diameter of each roll is 10 mm. Such a small diameter allows the roll to rotate around its own bending axis. The power source is a three-phase asynchronous motor, which makes the work rolls rotate synchronously and reversely. The width of the sheet that can be formed with this equipment is more than 500 mm.

Figure 11. Experimental equipment for continuous roll forming.

In order to verify the validity of the modified formulas, convex and saddle surfaces with a transversal curvature radius of 800 mm and a compression ratio of 5% are formed. The theoretical values of the longitudinal curvature radius are calculated by the formulas before and after modification, respectively, and compared with the actual forming results. The formed convex part and saddle part are shown in Figure 12. It can be seen that the forming effect of three-dimensional parts is good and there are no wrinkles, dimples or other defects.
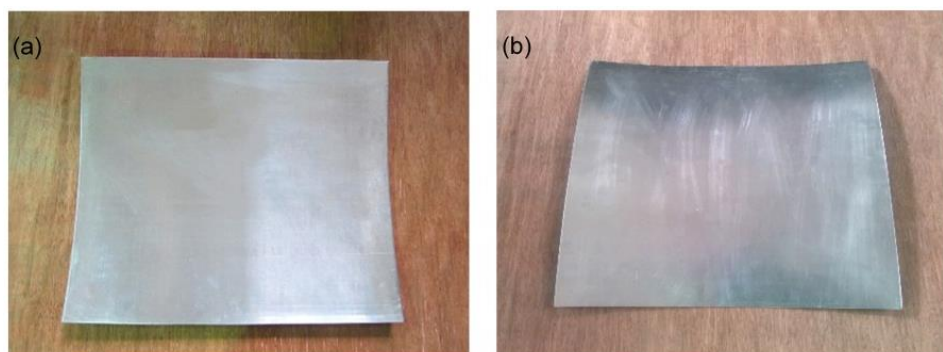

Figure 12. Formed parts by the continuous roll forming (CRF) equipment: (**a**) convex surface; (**b**) saddle surface.

4.2. Analysis of Experimental Results

The three-dimensional point cloud of the experimental part is obtained by a binocular stereo vision measurement device. The difference between the actual forming part and the target part can be compared by importing the point cloud into the reverse engineering software Geomagic Qualify. The profiles at different positions in the transversal and longitudinal directions are taken for analysis. Figure 13 shows the location of different profiles of convex and saddle surfaces. Among them, BB1, AA1, and CC1 correspond to $x = 0$ and $x = \pm 100$ mm, respectively, while DD1 and EE1 correspond to $y = 0$ and $y = -90$ mm, respectively. The normal absolute errors can be seen from Figure 14, in which AA1*~EE1* indicate the errors before modification, and AA1~EE1 show the errors after modification.

Figure 14 indicates that the normal absolute errors of longitudinal profiles DD1 and EE1 are significantly reduced after correction. The error range of DD1 for convex surface is reduced from 0.0583~7.9917 mm to −1.1956~2.9969 mm, and the error range of EE1 is changed from 0.9971~10.4136 mm to −0.2572~5.1413 mm. For saddle surface, the error range of DD1 is reduced from −0.1509~4.7866 mm to −2.2852~1.8914 mm, and that of EE1 is changed from 1.5844~5.6089 mm to 0.0699~3.2534 mm. The decrease in error fluctuation illustrates that the forming results are more stable. It can also be seen from the figure that the errors of the transversal profiles are prominently reduced, and the transversal error at each position after correction is controlled within 3.7260 mm for convex surfaces and 3.8668 mm for saddle surfaces. Similarly to the simulation results, the error in the end region is larger than that

in the middle region. The above error sources may be the elastic deformation of the rolls and the imprecise adjustment of the roll gap.
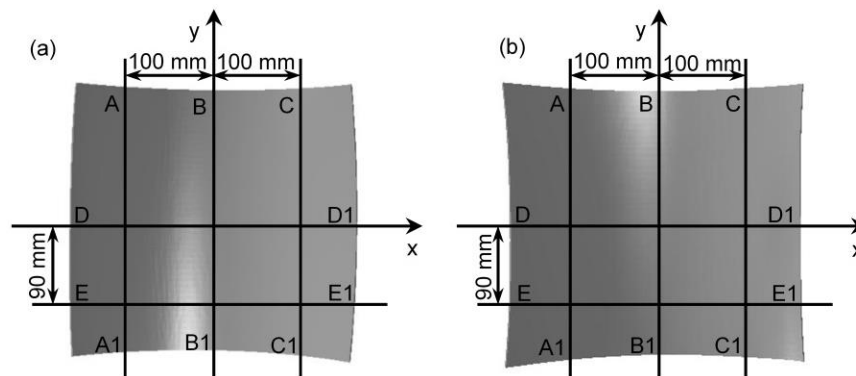

Figure 13. Different measuring positions of 3D surfaces: (**a**) convex surface; (**b**) saddle surface.
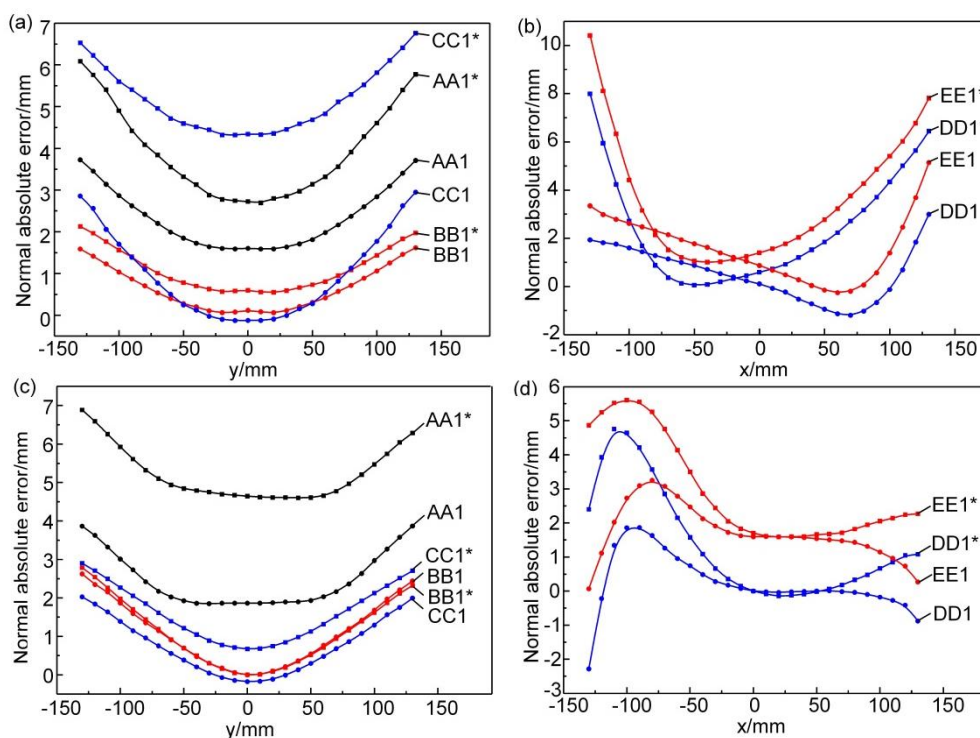

Figure 14. Normal absolute errors for 3D surfaces (A superscript asterisk indicates before correction): (**a**) transversal profiles of convex surface; (**b**) longitudinal profiles of convex surface; (**c**) transversal profiles of saddle surface; (**d**) longitudinal profiles of saddle surface.

5. Conclusions

CRF is a new technology for forming 3D curved surface in recent years. In order to predict the longitudinal curvature radius of the sheet in this process more accurately, the theoretical derivation is carried out, and the applicability of the formulas is verified by the numerical simulation and experimental analysis. The specific conclusions can be summarized as follows:

(1)   The principle of CRF is discussed, and the mechanism of longitudinal bending of sheet metal in the forming process is explained. It is proposed that the longitudinal strain of sheet metal can be divided into not only membrane strain and first-order bending strain, but also a secondary-order compensation strain which together with bending strain determines the longitudinal curvature of the sheet.

(2) The formulas for calculating the longitudinal curvature radius of convex and saddle surfaces with the range of transversal curvature radii of 800~1000 mm and compression ratios of 3~7% are derived, and the mathematical equations of the convex and saddle surfaces to be formed are given.

(3) The roll gap is the key factor to determine the forming quality and precision of 3D surface in CRF. When the roll gap is small in the middle and large on both sides, the sheet metal is bent upward to form a convex surface, and a saddle surface will be formed if the distribution of the roll gap is the opposite. According to the new calculation formulas of longitudinal curvature radius, the design method of the roll gap for convex and saddle surfaces is deduced, and the roll gap dimensions at different positions are quantitatively given based on the new method.

(4) The superiority of the new formulas is verified by numerical simulation. From the numerical simulation results, it is found that for convex surfaces, the error of the longitudinal centerline is reduced from 13.67%, 13.26% and 11.11% to 4.35%, 5.50% and 3.49% when the transversal curvature radius is 800 mm and the compression ratios are 5%, 6% and 7%, respectively. For saddle-shaped parts, when the compression ratio is 5% and the transversal curvature radii are 800, 850 and 900 mm, respectively, the error of the longitudinal centerline is reduced from the original 6.81%, 7.02%, and 13.53% to 0.41%, 0.28% and 6.83%, respectively.

(5) The viewpoint of this paper is further verified by the CRF experiment. When the transversal curvature radius is 800 mm and the compression ratio is 5%, the normal absolute error ranges of the profile at 90 mm from longitudinal centerline (y = −90 mm) for convex and saddle surfaces are reduced from 0.9971~10.4136 mm and 1.5844~5.6089 mm before modification to −0.2572~5.1413 mm and 0.0699~3.2534 mm after modification, which shows that the new calculation formulas of longitudinal curvature radius are of great significance for continuous roll forming.

Author Contributions: Conceptualization, J.G., Z.C. and L.S.; methodology, J.G. and Z.C.; software, J.G. and X.Z.; validation, J.G., Z.C. and D.H.; investigation, J.G., Z.C. and D.H.; writing—original draft preparation, J.G.; writing—review and editing, J.G. and D.H.; funding acquisition, Z.C. All authors have read and agreed to the published version of the manuscript.

Conflicts of Interest: The authors declare no conflict of interest.

References

1. Abebe, M.; Park, J.W.; Kim, J.; Kang, B.S. Numerical verification on formability of metallic alloys for skin structure using multi-point die-less forming. *Int. J. Precis. Eng. Manuf.* **2017**, *18*, 263–272.

2. Kim, D.K.; Park, D.K.; Kim, J.H.; Kim, S.J.; Kim, B.J.; Seo, J.K.; Paik, J.K. Effect of corrosion on the ultimate strength of double hull oil tankers—Part I: Stiffened panels. *Struct. Eng. Mech.* **2012**, *42*, 507–530. [CrossRef]

3. Saidi, B.; Moreau, L.G.; Mhemed, S.; Cherouat, A.; Adragna, P.-A.; Nasri, R. Hot incremental forming of titanium human skull prosthesis by using cartridge heaters: A reverse engineering approach. *Int. J. Adv. Manuf. Technol.* **2019**, *101*, 873–880. [CrossRef]

4. Waldmann, D.; May, A.; Thapa, V.B. Influence of the sheet profile design on the composite action of slabs made of lightweight woodchip concrete. *Constr. Build. Mater.* **2017**, *148*, 887–899. [CrossRef]

5. Li, M.Z.; Cai, Z.Y.; Sui, Z.; Yan, Q.G. Multi-point forming technology for sheet metal. *J. Mater. Process. Technol.* **2002**, *129*, 333–338. [CrossRef]

6. Xing, J.; Li, M.Z.; Cheng, Y.Y.; Wang, B.L.; Yang, Z.; Wang, Y. Effect of the arrangement of the punch units in multi-point stretch forming process. *Int. J. Adv. Manuf. Technol.* **2016**, *86*, 2309–2317. [CrossRef]

7. Yu, J.Q.; Li, Y.; Teng, F.; Liang, J.C.; Lin, X.F.; Liang, C.; Chen, G.Y.; Sun, G.P. Research on the cross section forming quality of three-dimensional multipoint stretch forming parts. *Adv. Mater. Sci. Eng.* **2018**, *2018*, 4265617. [CrossRef]

8. Tsuji, N.; Saito, Y.; Utsunomiya, H.; Tanigawa, S. Ultra-fine grained bulk steel produced by accumulative roll-bonding (ARB) process. *Scr. Mater.* **1999**, *40*, 795–800. [CrossRef]

9.   Lin, Y.H.; Hua, M. Influence of strain hardening on continuous plate roll-bending process. *Int. J. Non-Linear Mech.* **2000**, *35*, 883–896. [CrossRef]

10.   Yoon, S.J.; Yang, D.Y. Development of a highly flexible incremental roll forming process for the manufacture of a doubly curved sheet metal. *CIRP Ann.-Manuf. Technol.* **2003**, *52*, 201–204. [CrossRef]

11.   Shim, D.S.; Yang, D.Y.; Kim, K.H.; Han, M.S.; Chung, S.W. Numerical and experimental investigation into cold incremental rolling of doubly curved plates for process design of a new LARS (line array roll set) rolling process. *CIRP Ann.-Manuf. Technol.* **2009**, *58*, 239–242.

12.   Cai, Z.Y.; Lan, Y.W.; Li, M.Z.; Hu, Z.Q.; Wang, M. Continuous sheet metal forming for doubly curved surface parts. *Int. J. Precis. Eng. Manuf.* **2012**, *13*, 1997–2003. [CrossRef]

13.   Cai, Z.Y.; Li, M.Z.; Lan, Y.W. Three-dimensional sheet metal continuous forming process based on flexible roll bending: Principle and experiments. *J. Mater. Process. Technol.* **2012**, *212*, 120–127. [CrossRef]

14.   Gong, X.P.; Li, M.Z.; Hu, Z.Q.; Cai, Z.Y. Research on continuous multi-point forming technology for three-dimensional sheet metal. *Int. J. Mater. Prod. Technol.* **2010**, *38*, 210–222. [CrossRef]

15.   Li, M.Z.; Cai, Z.Y.; Li, R.J.; Lan, Y.W.; Qiu, N.J. Continuous forming method for three-dimensional surface parts based on the rolling process using bended roll. *J. Mech. Eng.* **2012**, *48*, 44–49. [CrossRef]

16.   Cai, Z.Y.; Li, M.Z. Mechanical mechanism of continuous roll forming for three-dimensional surface parts and the calculation of bending deformation. *J. Mech. Eng.* **2013**, *49*, 35–41.

17.   Li, R.J.; Li, M.Z.; Qiu, N.J.; Cai, Z.Y. Surface flexible rolling for three-dimensional sheet metal parts. *J. Mater. Process. Technol.* **2014**, *214*, 380–389.

18.   Liu, P.; Ku, T.W.; Kang, B.S. Shape error prediction and compensation of three-dimensional surface in flexibly-reconfigurable roll forming. *J. Mech. Sci. Technol.* **2015**, *29*, 4387–4397. [CrossRef]

19.   Liu, K.; Fu, W.Z.; Li, M.Z.; Li, Y.; Yi, Z. Research on flexible rolling process of three-dimensional surface part using auxiliary rolls. *Int. J. Adv. Manuf. Technol.* **2019**, *103*, 1433–1442. [CrossRef]

20.   Park, J.W.; Kang, B.S. Comparison between regression and artificial neural network for prediction model of flexibly reconfigurable roll forming process. *Int. J. Adv. Manuf. Technol.* **2019**, *101*, 3081–3091.

21.   Ghiabakloo, H.; Park, J.W.; Kil, M.G.; Lee, K.; Kang, B.S. Design of the flexibly-reconfigurable roll forming process by a progressively-improving goal seeking approach. *Int. J. Mech. Sci.* **2019**, *157–158*, 136–149. [CrossRef]

22.   Cai, Z.Y.; Li, M.Z. Principle and theoretical analysis of continuous roll forming for three-dimensional surface parts. *Sci. China-Technol. Sci.* **2013**, *56*, 351–358. [CrossRef]

23.   Cai, Z.Y.; Wang, M.; Li, M.Z. Study on the continuous roll forming process of swept surface sheet metal part. *J. Mater. Process. Technol.* **2014**, *214*, 1820–1827. [CrossRef]

24.   Cai, Z.Y.; Guan, D.B.; Wang, M.; Li, M.Z. A novel continuous roll forming process of sheet metal based on bended rolls. *Int. J. Adv. Manuf. Technol.* **2014**, *73*, 1807–1814. [CrossRef]